Available online at www.sciencedirect.com
ScienceDirect
Nuclear Instruments and Methods in Physics Research A 571 (2007) 207–210
NUCLEAR INSTRUMENTS & METHODS IN PHYSICS RESEARCH Section A
www.elsevier.com/locate/nima

Count rate performance study of the Lausanne ClearPET scanner demonstrator ☆

M. Rey[a,*], S. Jan[b], J.-M. Vieira[a], J.-B. Mosset[a], M. Krieguer[c], C. Comtat[b], C. Morel[d]

[a]*LPHE, Ecole Polytechnique Fédérale de Lausanne, CH-1015 Lausanne, Switzerland*
[b]*Service Hospitalier Frédéric Joliot, CEA, F-91401 Orsay, France*
[c]*IIHE, Vrije Universiteit Brussel, B-1050 Brussels, Belgium*
[d]*CPPM, CNRS-IN2P3, Université de la Méditerranée Aix-Marseille II, F-13288 Marseille, France*

Available online 7 November 2006

Abstract

This paper presents the count rate measurements obtained with the Lausanne partial ring ClearPET scanner demonstrator and compares them against GATE Monte Carlo simulations. For the present detector setup, a maximum single event count rate of 1.1 Mcps is measured or a 250–750 keV energy window. This corresponds to a coincidence count rate of approximately 22 kcps. Good agreements are observed between measured and simulated data. Count rate performance, including Noise Equivalent Count (NEC) curves, are determined and extrapolated for a full ring ClearPET design using GATE Monte Carlo simulations. For a full ring design with three rings of detector modules, NEC is peaking at about 70 kcps for 20 MBq.

PACS: 87.58.Fg; 24.10.Lx

Keywords: PET; ClearPET; DOI; Monte Carlo; GATE; Small animal imaging

1. Introduction

Positron Emission Tomography (PET) applied to small animal imaging is a potentially important tool in developing new drugs and imaging gene expression. The Crystal Clear Collaboration (CCC) [1] is developing a new family of small animal PET scanners called ClearPET, which is based on LSO/LuYAP Depth-Of-Interaction (DOI) sensitive detector modules. In parallel, GATE, a new Monte Carlo simulator based on Geant4 was developed to help in the design of the ClearPET prototypes [2]. Count rate measurements obtained with the Lausanne ClearPET scanner demonstrator are presented and compared against GATE Monte Carlo simulations.

2. Material and methods

2.1. Detector setup

The Lausanne ClearPET scanner demonstrator contains six sectors of three rings of LSO/LuYAP detector modules with an inner ring diameter of 14.1 cm. Each detector module consists of a double layer phoswich array of 8×8 pixels optically coupled with a Multi-anode Photo-Multiplier Tube (MaPMT) Hamamatsu R7600-M64. Every crystal measures $2.0 \times 2.0 \times 8.0\,\text{mm}^3$. The crystal pitch is 2.3 mm to match the pitch of the MaPMT channels [3].

The gantry that holds the detectors allows for rotating continuously over 360°. Slip rings are used to transmit signals and to empower electronics embedded in the rotating part of the gantry. For all acquisitions, the gantry was rotated at a constant angular speed of 1 rpm. Two against four sectors were mounted asymmetrically, so that only two sectors are facing exactly each other. This geometry allows to scan the full Field-Of-View (FOV),

☆ This work was supported by the Swiss National Science Foundation under Grant nos. 2153-063870 and 205320-100472.
*Corresponding author.
E-mail address: martin.rey@epfl.ch (M. Rey).

0168-9002/$ - see front matter © 2006 Elsevier B.V. All rights reserved.
doi:10.1016/j.nima.2006.10.064

even though a partial ring configuration is employed. The same geometry was used for GATE simulations.

2.2. Data acquisition and Monte Carlo simulations

Data acquisition is based on 40 MHz FPGA-based free-running sampling electronics [4]. A master–slave data acquisition software described in Ref. [5] is used. Singles are stored in a dedicated list-mode format, which is also used to store singles generated by GATE. Furthermore, the Monte Carlo history of a simulated event is stored in an extra record attached to the event. This information is used to identify scattered coincidences, for which at least one of the annihilation photons encountered a Compton interaction in the phantom.

Both for the measured and simulated data, coincidences are associated off-line by the software using a 10 ns time window and also stored in the list-mode format as for singles. Randoms are estimated by adding increasingly to every sector of modules an extra 100 ns time delay. Like it was shown in Ref. [6], full combinatorial statistics of multiple coincidences are recorded for both the prompt and delayed coincidences, in order to estimate accurately the rates of true coincidences by subtracting rates of delayed from prompt coincidences.

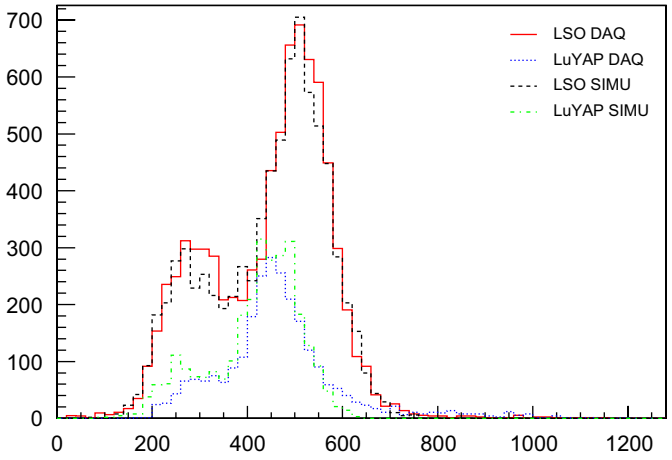

Fig. 1. Validation of the energy spectra of a given module. LSO and LuYAP spectra are shown and superimposed with simulated spectra obtained with GATE.

3. Results and discussion

3.1. Energy spectra

With the aim to simulate the ClearPET demonstrator as accurately as possible, we paid special attention to the digitization of the detector modules. For this, energy

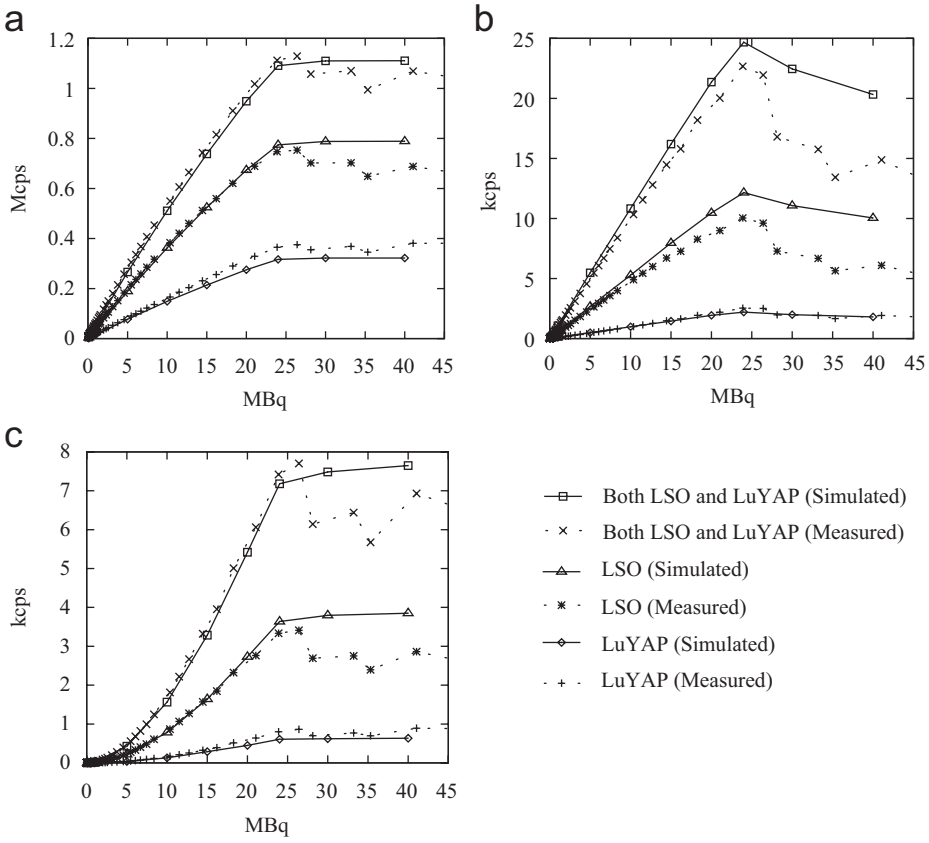

Fig. 2. Comparison between DAQ and simulated count rates for a three partial ring ClearPET. Low density LuYAP crystals were simulated: (a) singles; (b) prompt coincidences; and (c) randoms coincidences.

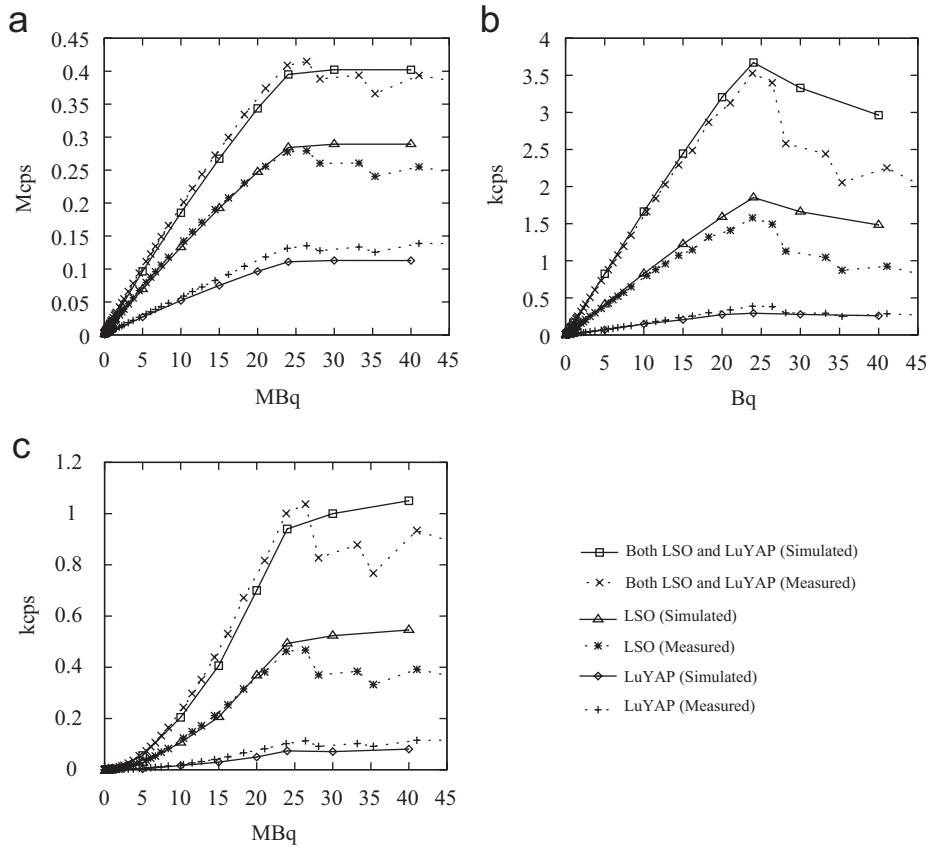

Fig. 3. Comparison between DAQ and simulated count rates for the central ring of the ClearPET. Low density LuYAP crystals were simulated: (a) singles; (b) prompt coincidences; and (c) randoms coincidences.

resolution, peak position at full energy and hardware threshold were modeled, according to the dispersion of these parameters measured with the experimental setup. Thus, simulated FWHM energy resolution, peak position at full energy and trigger efficiency are randomly distributed for every detector module using Gaussian blurs. FWHM energy resolutions of modules were blurred around $(31 \pm 7)\%$ for LSO and $(34 \pm 1)\%$ for LuYAP. Similarly, peak positions at full energy were distributed around (500 ± 70) keV for LSO and (490 ± 60) keV for LuYAP. Finally, trigger efficiencies were modeled by sigmoid functions $s(E)$ as given by Eq. (1), where the threshold value E_0 was randomly distributed for each detector module around (180 ± 50) keV and the slope factors α around $(0.05 \pm 0.01)\,\mathrm{keV}^{-1}$.

$$s(E) = \frac{1}{1 + e^{-\alpha(E-E_0)}}. \quad (1)$$

Fig. 1 shows the LSO and LuYAP spectra for simulated and acquired data for a given pixel.

3.2. Count rate performances

Count rate curves were obtained with a cylindrical phantom filled with [F-18] FDG. A set of 1 min scans was acquired every half hour for almost 24 h.

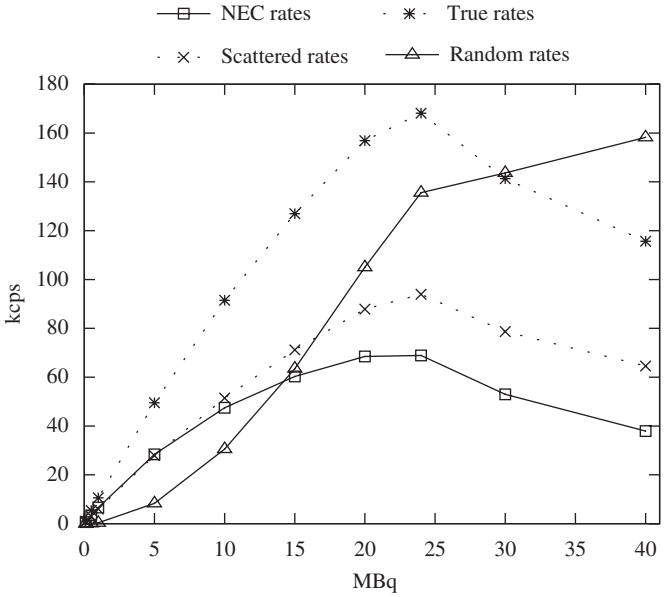

Fig. 4. Simulated NEC curves for a full ring design with three rings of detector modules composed with LSO and low density LuYAP crystals.

The simulations were performed with two different $Lu_xY_{1-x}AP$ crystal densities, as used in the ClearPET demonstrator: high density $Lu_{0.7}Y_{0.3}AP$ of $7.1\,g/cm^3$ and low density $Lu_{0.45}Y_{0.55}AP$ of $6.6\,g/cm^3$. As measured for the ClearPET detector modules, we used a FWHM time

resolution of 3.4 ns for LSO and 3.75 ns for LuYAP. To account for free-sampling electronics dead-times, we simulated non-paralyzing dead-times of 400 ns per detector module and 700 ns per sector (each sector comprises three detector modules). A buffering model was implemented to account for the readout of the digital I/O data acquisition boards. Finally, a random rejection of 7% of the single events was applied to account for multiple triggers within detector modules.

Figs. 2–4 take into account only the simulations for tomographs composed with low density LuYAP crystals. The count rates for high density LuYAP tomographs are slightly higher.

As shown in Figs. 2(a) and (c), singles and random count rates are quite well reproduced, whereas the prompt coincidence count rates (Fig. 2(b)) are a bit lower than the simulated ones. However, the corresponding count rates determined for the central ring of detector modules only match better together (Fig. 3). This is consistent with the fact that the cylinder was not perfectly centred axially, whereas the simulated phantom was.

The Fig. 4 shows the Noise Equivalent Count (NEC) curves calculated using Eq. (2) [7] from the simulated count rates of a full ring design with three rings of detector modules, where T are the trues, S the scattered and R the randoms coincidence count rates and f is the ratio between the phantom and the detector ring diameters.

$$\mathrm{NEC}(T,S,R)=\frac{T^2}{T+S+2fR}. \quad (2)$$

The NEC peak estimated by GATE for a full ring design with three rings of detector modules amounts to about 70 kcps at 20 MBq. At NEC maximum, the scatter fraction, $\mathrm{SF}=S/(T+S)$, is about 36% and the random fraction, $\mathrm{RF}=R/(T+S+R)$, 30%.

4. Conclusion

Results obtained with the Lausanne ClearPET demonstrator show a good agreement between the measurements and the simulations. The impact on NEC performance of the use of high density versus low density LuYAP crystals in the LSO/LuYAP phoswich modules appears to be rather weak, since most of the annihilation photons interact in the LSO layer of the detector. Further studies following this validation of the modeling of the ClearPET demonstrator by GATE will allow to define an optimal design for LSO/LuAP phoswich arrangements with regards to detector sensitivity and image spatial resolution.

References

[1] K. Ziemons, E. Auffray, R. Barbier, et al., Nucl. Instr. and Meth. A 537 (2005) 307.
[2] S. Jan, G. Santin, D. Strul, et al., Phys. Med. Biol. 49 (2004) 4543.
[3] J.-B. Mosset, O. Devroede, M. Krieguer, et al., IEEE Trans. Nucl. Sci. NS-53 (2006) 25.
[4] M. Streun, G. Brandenburg, H. Larue, et al., IEEE Trans. Nucl. Sci. NS-48 (2001) 524.
[5] M. Rey, J.-M. Vieira, J.-B. Mosset, et al., Measured and simulated specifications of the Lausanne ClearPET Scanner Demonstrator, in: Nuclear Science Symposium, vol. 4, IEEE, New York, 2005, p. 2070.
[6] L. Simon, D. Strul, G. Santin, et al., Nucl. Instr. and Meth. A 527 (2004) 190.
[7] M.E. Daube-Witherspoon, J.S. Karp, M.E. Casey, et al., J. Nucl. Med. 43 (10) (2002) 1398.